J. Fluid Mech. (2002), *vol.* 456, *pp.* 199–218.
DOI: 10.1017/S0022112001007571 Printed in the United Kingdom

The stability and transition of the boundary layer on a rotating sphere

By S. J. GARRETT[1] AND N. PEAKE[2]

[1]Department of Engineering, University of Cambridge, Trumpington Street, Cambridge CB2 1PZ, UK

[2]Department of Applied Mathematics and Theoretical Physics, University of Cambridge, Silver Street, Cambridge CB3 9EW, UK

(Received 3 May 2001 and in revised form 21 August 2001)

This paper is concerned with convective and absolute instabilities in the boundary-layer flow over the outer surface of a sphere rotating in an otherwise still fluid. Viscous and streamline-curvature effects are included and the analysis is conducted between latitudes of 10° and 80° from the axis of rotation. Both convective and absolute instabilities are found at each latitude within specific parameter spaces. The results of the convective instability analysis show that a crossflow instability mode is the most dangerous below $\theta = 66°$. Above this latitude a streamline-curvature mode is found to be the most dangerous, which coincides with the appearance of reverse flow in the radial component of the mean flow. At low latitudes the disturbances are considered to be stationary, but at higher latitudes they are taken to rotate at 76% of the sphere surface speed, as observed in experimental studies. Our predictions of the Reynolds number and vortex angle at the onset of convective instability are consistent with existing experimental measurements. Results are also presented that suggest that the occurrence of the slowly rotating vortices is associated with the dominance of the streamline-curvature mode at $\theta = 66°$. The local Reynolds number at the predicted onset of absolute instability matches experimental data well for the onset of turbulence at $\theta = 30°$; beyond this latitude the discrepancy increases but remains relatively small below $\theta = 70°$. It is suggested that this absolute instability may cause the onset of transition below $\theta = 70°$. Close to the pole the predictions of each stability analysis are seen to approach those of existing rotating disk investigations.

1. Introduction

When a sphere rotates in still fluid a flow is induced in which the fluid moves over the outer surface from the poles to the equator and is ejected radially from the equator. The resulting three-dimensional flow was first investigated theoretically by Howarth (1951), who made boundary-layer approximations to the steady Navier–Stokes equations and used a series solution to calculate the mean flow. Theoretical papers in the past have concentrated on the laminar mean flow, and for instance Banks (1965) uses Howarth's series solution and Manohar (1967) and Banks (1976) use more accurate finite difference techniques. The experimental papers of Sawatzki (1970) and Kohama & Kobayashi (1983) report that the flow exhibits transitional and turbulent regions as well as the laminar region. The flow around the pole remains laminar, with spiral vortices characteristic of crossflow instabilities appearing at a higher latitude, while the turbulent region occurs after the vortices have broken

down at a higher latitude still. The results of Kohama & Kobayashi show that the onset of transition to turbulence occurs at a repeatable consistent local Reynolds number that is roughly the same at all latitudes below $\theta = 70^\circ$, despite the instability waves first appearing across a wide parameter range with varying rotation rate and sphere radius. This observation is highly suggestive that the boundary layer becomes absolutely unstable at, or just before, the transition location, leading to the temporal growth of the disturbances at that point and triggering the nonlinear behaviour characteristic of the onset of transition. This is precisely the mechanism which has been claimed by Lingwood (1995) to pertain to transition on the rotating disk. Given the similarity between the boundary layers on the rotating disk and the sphere, it is reasonable to expect that the sphere might exhibit absolute instability as well, and this is what will be investigated here. The experimental papers of Sawatzki (1970) and Kohama & Kobayashi (1983) also report that the transitional and turbulent regions move nearer to the pole with increased rotation rate. The spiral vortices are observed to make an angle of 14° to a circle parallel to the equator at the onset of instability, which reduces to around 4°–8° as the rotation rate is increased. The number of spiral vortices at the onset of instability increases with increased rotation rate and appears to asymptotically approach a value of 31 or 32, which is the same number as observed experimentally on the rotating disk.

The transition of the boundary layer on a rotating sphere is also studied in the experimental paper of Kobayashi & Arai (1990). For rotating disks and cones experiments have shown that the spiral vortices are fixed on the body's surface at all times, see Kohama (1984) and Kobayashi *et al.* (1987). However, Kobayashi & Arai observe that the spiral vortices are fixed on the sphere surface when the rotation rate is large, while they move relative to the sphere surface when the rotation rate is small. The relative speed of these slow vortices is always 0.76 times the surface speed of the sphere. For zero axial flow, the slow vortices occur below a spin Reynolds number of approximately 10^5.

To our knowledge the only theoretical paper on the stability of the rotating-sphere boundary layer is by Taniguchi, Kobayashi & Fukunishi (1998). The paper uses linear stability theory, as we do in this paper although by taking a different approach, to predict the onset of convective instability and hence the appearance of the spiral vortices on a sphere rotating in an otherwise still fluid. The perturbation equations derived in their paper are solved at each latitude using the approximate mean flow profiles of Banks (1965). Taniguchi *et al.* show that both crossflow and streamline-curvature instabilities appear in the boundary layer. The two instability types correspond to the appearance of two lobes on the neutral curves. The crossflow instability dominates near to the poles and the streamline-curvature instability dominates near to the equator. The number of vortices at the onset of instability is also calculated at each latitude and is seen to decrease with increasing latitude. At the onset of instability the spiral vortices are predicted to be stationary with respect to the sphere surface, with the region of instability moving closer to the pole with increased rotation rate. The discrepancy between the experimental critical Reynolds numbers for the onset of spiral vortices and those calculated increases slightly with latitude when below 70° but still shows reasonably good agreement. However, above a latitude of 70° the predicted critical Reynolds numbers diverge sharply from the experimental values.

If the response to a transient disturbance is unbounded for large time at all points in space, the flow is absolutely unstable. If the boundary layer were solely convectively unstable a purely spatial analysis would be appropriate, but if the flow becomes absolutely unstable, then unless a spatio-temporal analysis is performed, important

characteristics will be missed. In this paper a spatial analysis is used to study the convective instability of the boundary layer in conditions when the flow is not absolutely unstable and then a spatio-temporal analysis is used to study the absolute instability of the rotating-sphere boundary layer. Briggs (1964) and Bers (1975) have shown that an absolute instability can be identified by singularities corresponding to zeros of the dispersion relation. The singularities occur when waves that propagate energy in different directions coalesce, with the point of coalescence known as a pinch point. Pinch points can appear as the Reynolds number is varied, and at these points the flow changes from a convectively unstable regime to an absolutely unstable regime. Examples of absolute instability in fluid mechanics include the work by Huerre & Monkewitz (1985), Niew (1993) and Lingwood (1995, 1997). Similar ideas have applied in the context of the boundary layer on a swept wing, see for example Taylor & Peake (1998). In this present paper, Briggs' method is used to distinguish between absolutely and convectively unstable time-asymptotic responses to impulsive excitation of the rotating-sphere boundary layer, closely following the work of Lingwood (1995) on the rotating disk. In § 2 the solution of the steady boundary-layer equations that give the laminar flow profiles is described and the unsteady perturbation equations for the system derived. The convective and absolute instability analyses are conducted in § 3 and § 4 respectively, where our theoretical predictions are compared with existing experimental results.

2. Formulation

We use a spherical polar coordinate system that is fixed in space with origin located at the centre of the sphere. The sphere is of radius $a^\star$ and rotates at a constant angular frequency $\Omega^\star$, the distance $r^\star$ is measured radially from the centre of the sphere, θ is the latitude measured from the axis of rotation and ϕ is the azimuth. The coefficient of kinematic viscosity is denoted by $\nu^\star$ (stars indicate dimensional quantities).

The non-dimensional mean flow variables are defined as

$$U(\eta,\theta)=\frac{U^\star}{\Omega^\star a^\star},\quad V(\eta,\theta)=\frac{V^\star}{\Omega^\star a^\star},\quad W(\eta,\theta)=\frac{W^\star}{(\nu^\star\Omega^\star)^{1/2}},\tag{2.1}$$

where U, V and W are the non-dimensional velocities in the θ-, ϕ- and $r^\star$-directions respectively and $\eta=(\Omega^\star/\nu^\star)^{1/2}(r^\star-a^\star)$ is the non-dimensional distance from the sphere surface in the radial direction. Note that this variable is scaled on the boundary-layer thickness $\delta^\star=(\nu^\star/\Omega^\star)^{1/2}$. Because the sphere rotates in an otherwise still fluid the mean pressure, $P^\star$, is a constant and so does not appear in the mean flow equations.

The equations that govern the mean flow are stated in, amongst others, Banks (1965) and are non-dimensionalized using (2.1) as

$$W\frac{\partial U}{\partial\eta}+U\frac{\partial U}{\partial\theta}-V^2\cot\theta=\frac{\partial^2U}{\partial\eta^2},\tag{2.2}$$

$$W\frac{\partial V}{\partial\eta}+U\frac{\partial V}{\partial\theta}+UV\cot\theta=\frac{\partial^2V}{\partial\eta^2},\tag{2.3}$$

$$\frac{\partial W}{\partial\eta}+\frac{\partial U}{\partial\theta}+U\cot\theta=0.\tag{2.4}$$

These equations are based on the usual boundary-layer assumption of large Reynolds

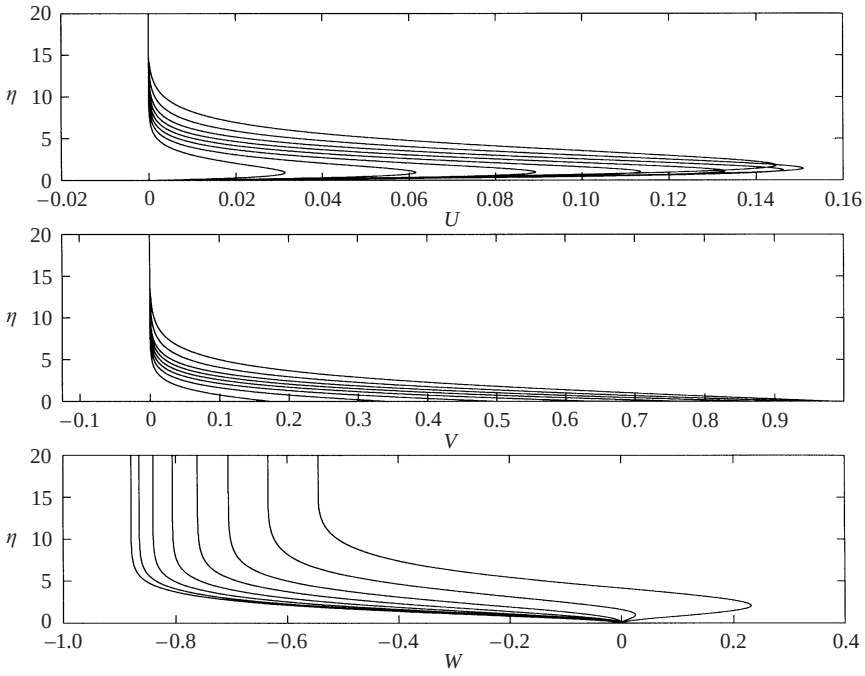

FIGURE 1. Mean velocity profiles $U(\eta)$, $V(\eta)$, $W(\eta)$ at latitudes of $\theta = 10°$–$80°$ (left to right) in $10°$ increments.

number. The non-dimensional boundary conditions are

$$\left.\begin{array}{ll} U = W = V - \sin\theta = 0, & \eta = 0, \\ U = V = 0, & \eta \to \infty. \end{array}\right\} \tag{2.5}$$

The first set represents the no-slip condition on the sphere surface, and the second set represents the quiescent fluid condition away from the sphere.

The system of equations (2.2)–(2.5) is solved using the NAG routine D03PEF to find the mean flow at each latitude. This NAG routine is a general PDE solver that reduces the system of PDEs to a system of ODEs in η. The resulting system of ODEs is solved at each latitude by marching from a given complete solution at $\theta = 5°$ towards the equator $\theta = 90°$ in $1°$ increments. At each latitude a backward differentiation formula method is used over a regularly spaced grid of 2000 data points between $\eta = 0$ and $\eta = 20$. The initial solution at $\theta = 5°$ is found using the series solution method as described by Banks (1965). The resulting profiles have been compared to the finite difference results of Banks (1976) and complete agreement is found up to the equator. Figure 1 shows the three velocity components at latitudes of $\theta = 10°$–$80°$ in $10°$ increments. Note that the latitudinal velocity, U, is inflectional at all latitudes, and also that fluid is entrained radially into the boundary layer at all the latitudes shown.

The stability analysis conducted at a particular latitude involves imposing infinitesimal small perturbations on the steady mean flow at that latitude. The dimensional perturbation variables (denoted by lower-case hatted quantities) are assumed to have the normal-mode form

$$(\hat{u}^\star, \hat{v}^\star, \hat{w}^\star, \hat{p}^\star) = (u^\star(r^\star), v^\star(r^\star), w^\star(r^\star), p^\star(r^\star))\mathrm{e}^{\mathrm{i}(\alpha^\star a^\star\theta + \beta^\star a^\star\phi\sin\theta - \gamma^\star t^\star)}. \tag{2.6}$$

The distance measured over the surface of the sphere from the pole to the latitude under consideration is $a^\star\theta$, and the dimensional wavenumber in this direction is $\alpha^\star$. The distance measured along a circular cross-section of the sphere by a plane perpendicular to the axis of rotation is $a^\star\phi\sin\theta$, and the dimensional wavenumber in this direction is $\beta^\star$. The perturbed flow variables are now substituted into the dimensional Navier–Stokes equations, with the perturbing quantities considered sufficiently small that the resulting perturbation equations can be linearized. The perturbing quantities are non-dimensionalized on the typical length, velocity, time and pressure scales: $\delta^\star$, $a^\star\Omega^\star$, $\delta^\star/a^\star\Omega^\star$ and $\rho^\star(a^\star\Omega^\star)^2$ respectively, where $\rho^\star$ is the fluid density. The mean-flow quantities are non-dimensionalized as in (2.1). This leads to a set of non-dimensional perturbation equations after $O(R^{-2})$ terms have been neglected. Here $R = \delta^\star a^\star\Omega^\star/\nu^\star$ is the Reynolds number. Factors $1/(1+\eta/R)$ appear multiplying terms in the perturbation equations. These factors are set to unity in an approximation that is similar to the parallel flow approximations made in many other boundary-layer investigations. The parallel flow approximation limits the analysis to a local analysis at each value of θ and its validity at low and high latitudes is discussed in § 5.

The perturbation equations can be written as a set of six first-order ordinary differential equations using the transformed dependent variables:

$$z_1(\eta;\alpha,\beta,\gamma;R,\theta) = (\alpha - \mathrm{i}\cot\theta/R)u + \beta v, \tag{2.7}$$

$$z_2(\eta;\alpha,\beta,\gamma;R,\theta) = (\alpha - \mathrm{i}\cot\theta/R)\mathrm{D}u + \beta \mathrm{D}v, \tag{2.8}$$

$$z_3(\eta;\alpha,\beta,\gamma;R,\theta) = w, \tag{2.9}$$

$$z_4(\eta;\alpha,\beta,\gamma;R,\theta) = p, \tag{2.10}$$

$$z_5(\eta;\alpha,\beta,\gamma;R,\theta) = (\alpha - \mathrm{i}\cot\theta/R)v - \beta u, \tag{2.11}$$

$$z_6(\eta;\alpha,\beta,\gamma;R,\theta) = (\alpha - \mathrm{i}\cot\theta/R)\mathrm{D}v - \beta \mathrm{D}u, \tag{2.12}$$

where D represents differentiation with respect to η. Writing $\alpha_1 = \alpha - [\mathrm{i}\cot\theta/R]_s$, these equations are

$$\mathrm{D}z_1 = z_2, \tag{2.13}$$

$$\begin{aligned}\left[\frac{\mathrm{D}z_2}{R}\right]_v = {} & \frac{1}{R}([\alpha^2+\beta^2]_v + \mathrm{i}R(\alpha U + \beta V - \gamma))z_1 \\ & + \left[\frac{Wz_2}{R}\right]_s + \left(\alpha_1 U' + \beta V' + \left[\frac{1}{R}(\alpha_1 U + \beta V)\right]_s\right) z_3 \\ & + \mathrm{i}\left(\alpha^2+\beta^2 - \left[\frac{\mathrm{i}\alpha\cot\theta}{R}\right]_s\right) z_4 - \left[\frac{V\cot\theta z_5}{R}\right]_s \\ & + \left[\frac{1}{R}\left(\left(\alpha_1\frac{\partial U}{\partial\theta} + \beta\frac{\partial V}{\partial\theta}\right)u - (\alpha_1 V - \beta U)v\cot\theta\right)\right]_s,\end{aligned} \tag{2.14}$$

$$\mathrm{D}z_3 = -\mathrm{i}\phi_1 - \left[\frac{2z_3}{R}\right]_s, \tag{2.15}$$

$$\begin{aligned}\mathrm{D}z_4 = {} & \left[\frac{\mathrm{i}Wz_1}{R}\right]_s - \left[\frac{\mathrm{i}z_2}{R}\right]_v + \left[\frac{2}{R}(Uu+Vv)\right]_s \\ & -\frac{1}{R}([\alpha^2+\beta^2]_v + \mathrm{i}R(\alpha U + \beta V - \gamma) + \mathrm{D}W_s)z_3,\end{aligned} \tag{2.16}$$

$$\mathrm{D}z_5 = z_6, \tag{2.17}$$

$$\left[\frac{\mathrm{D}z_6}{R}\right]_v = \left[\frac{V\cot\theta z_1}{R}\right]_s + \left(\alpha_1\frac{\partial V}{\partial\eta} - \beta\frac{\partial U}{\partial\eta} + \left[\frac{1}{R}(\alpha_1 V - \beta U)\right]_s\right) z_3 + \left[\frac{Wz_6}{R}\right]_s + \left[\frac{1}{R}\left(\left(\alpha_1\frac{\partial V}{\partial\theta} - \beta\frac{\partial U}{\partial\theta}\right)u + (\alpha_1 U + \beta V)v\cot\theta\right)\right]_s + \left[\frac{\beta\cot\theta z_4}{R}\right]_s + \frac{1}{R}([\alpha^2+\beta^2]_v + \mathrm{i}R(\alpha U + \beta V - \gamma))z_5. \tag{2.18}$$

The subscripts v and s indicate which of the $O(R^{-1})$ terms arise from the viscous and streamline-curvature effects respectively. For a detailed investigation into streamline-curvature instability in three-dimensional boundary layers the interested reader is referred to Ito (1996). Note that since a stationary frame of reference is used Coriolis terms do not appear in (2.13)–(2.18). Note also that the perturbation velocities u and v still appear explicitly in (2.13)–(2.18), but can be expressed in terms of z_1 and z_2 via

$$u = \frac{1}{\alpha_1^2+\beta^2}(\alpha_1 z_1 - \beta z_5),$$

$$v = \frac{1}{\alpha_1^2+\beta^2}(\alpha_1 z_5 + \beta z_1).$$

The wavenumber in the θ-direction, α, and frequency, γ, are in general complex, as required by the spatio-temporal analysis of § 4; we write these quantities as $\alpha = \alpha_r + \mathrm{i}\alpha_i$ and $\gamma = \gamma_r + \mathrm{i}\gamma_i$. In contrast, the azimuthal wavenumber, β, is real. The angle that the phase fronts make with a circle parallel to the equator is denoted ϵ, and is found from

$$\epsilon = \tan^{-1}(\beta/\alpha_r). \tag{2.19}$$

The integer number of complete cycles of the disturbance round the azimuth is

$$n = \beta R\sin\theta. \tag{2.20}$$

Later in the paper, we will identify ϵ and n as being the angle and number of spiral vortices on the sphere surface.

By neglecting the $O(R^{-1})$ streamline-curvature terms in (2.13)–(2.18) we find the Orr–Somerfeld equation for the rotating sphere in the form

$$[\mathrm{i}(\mathrm{D}^2-\sigma^2)^2 + R(\alpha U + \beta V - \gamma)(\mathrm{D}^2-\sigma^2) - R(\alpha\mathrm{D}^2U + \beta\mathrm{D}^2V]z_3 = 0, \tag{2.21}$$

where $\sigma^2 = \alpha^2+\beta^2$.

3. The convective instability analysis

In this section we solve the eigenvalue problem defined by (2.13)–(2.18), with the homogenous boundary conditions

$$\left.\begin{array}{ll} z_i = 0, & \eta = 0, \\ z_i \to 0, & \eta \to \infty, \end{array}\right\} \tag{3.1}$$

where $i = 1, 2 \ldots 6$. This eigenvalue problem will be solved for certain combinations of values of α, β and γ at each Reynolds number, R, and for a particular value of θ. From these we form the dispersion relation, $\mathrm{D}(\alpha,\beta,\gamma;R,\theta) = 0$, at each θ, with the aim of studying the occurrence of convective instabilities. This allows a discussion

of the spatial branches of the dispersion relation before we study their pinching in the absolute instability analysis of § 4. In each analysis the branches were calculated using a double-precision fixed-step-size, fourth-order Runge–Kutta integrator with Gram–Schmidt orthonormalization and a Newton–Raphson linear search procedure, using a numerical code supplied by R. J. Lingwood (personal communication, 1999).

Since we are supposing here that the flow is not absolutely unstable it follows that in the Briggs–Bers procedure we can reduce the imaginary part of the frequency to zero, so that $\gamma_i = 0$. To produce the neutral curves for convective instability a number of approaches can be taken. One approach involves finding the region of convective instability at each latitude for different fixed vortex angles, so that β is known in terms of α from (2.19). For a particular θ the real part of the complex frequency, γ_r, and α are calculated with the perturbation equations solved for neutral stability, $\gamma_i = 0$, at each Reynolds number. This was the approach taken by Taniguchi *et al.* (1998) in their temporal analysis. Another approach is to insist that the vortices rotate at some fixed multiple of the sphere surface velocity, thereby fixing the ratio γ_r/β, and then α and β are calculated using a spatial analysis. This is the approach taken here. The non-dimensional speed of the surface of the sphere is $\sin\theta$, and equating the relevant multiple of this with the disturbance phase velocity in the same direction, γ_r/β, leads to $\gamma_r = c\beta\sin\theta$. This relationship must be satisfied with $c = 1.0$ if the vortices are to rotate with the sphere and $c = 0.76$ if the vortices are those reported by Kobayashi & Arai (1990) at high latitudes.

At the end of this section a further approach is taken in which the neutral curves are plotted at each latitude for various integer n. The global neutral curve at a particular latitude is then the envelope of the neutral curves pertaining to each single n. This method enables a prediction of the speed of the spiral vortices with respect to the sphere surface rather than making *a priori* assumptions on the longitudinal wave speed.

3.1. *Stationary vortices*

We begin by considering vortices that rotate with the surface of the sphere. Latitudes in the range $\theta = 10^\circ$–80° have been analysed in increments of 10°, and two spatial branches were found to determine the convective instability characteristics of the system at each latitude. Figure 2 shows these spatial branches in the complex α-plane at $\theta = 10^\circ$ and $R = 2400$. A branch lying below the α_r-axis indicates convective instability. In the analysis of the Orr–Somerfeld equation (2.21) branch 2 is not found, showing that it arises here from the effects of streamline curvature. This is consistent with existing work on the rotating disk, see Lingwood (1995). Figure 3 shows the two branches at $R = 2500$, where we see that an exchange of modes has occurred between them. The modified branch 1 now determines the regions of convective instability. Increasing the value of R causes the peak between the two minima on branch 1 to move downwards and the points where the branch crosses the α_r-axis move apart, thereby widening the regions of instability and mapping out two lobes on the neutral curve. Above a certain value of R the peak moves below the real α-axis and further increases in R change the region of instability, producing the upper and lower branches of the neutral curve. This branch behaviour is typical for all latitudes below $\theta = 66^\circ$. Above $\theta = 66^\circ$ the two branches only appear like those described when the peak in the modified branch 1 has moved below the α_r-axis after the branch exchange. The neutral curves for latitudes above $\theta = 66^\circ$ therefore do not have the two-lobed structure. At $\theta = 66^\circ$ a region of reverse flow first forms in the radial velocity component close to the sphere surface.

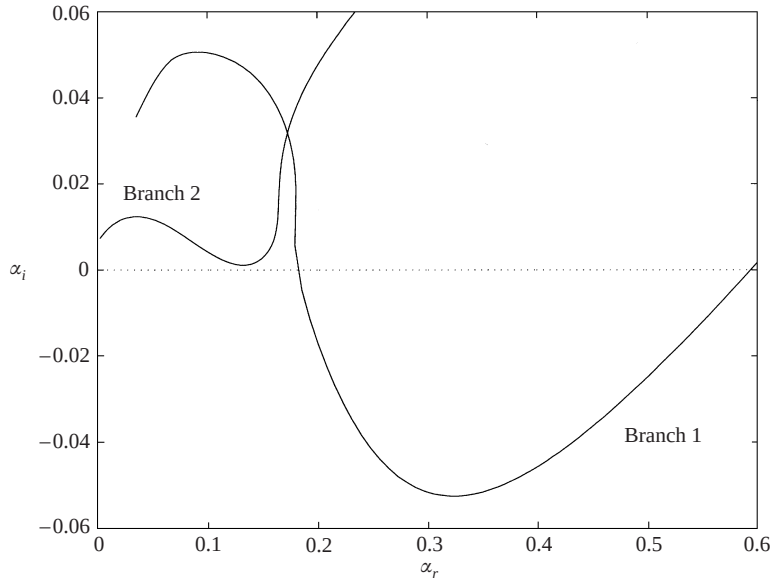

FIGURE 2. The two spatial branches at $\theta = 10^\circ$ and $R = 2400$ showing convective instability from branch 1 only.

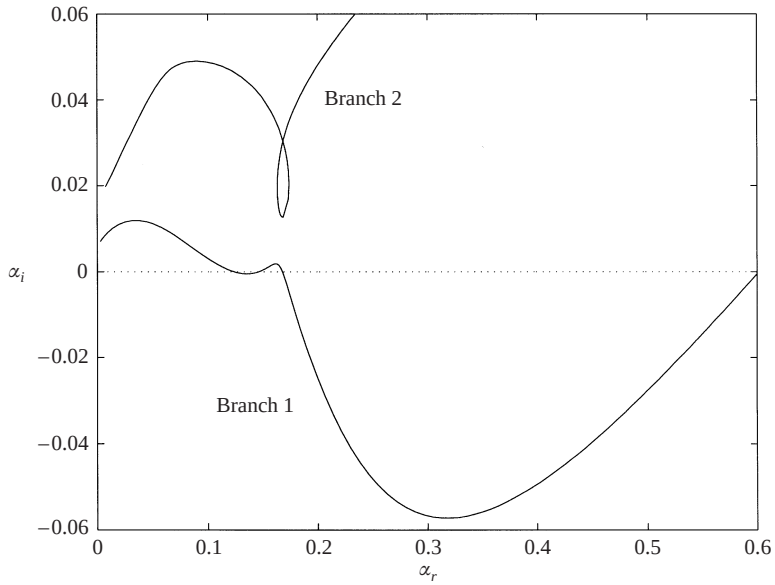

FIGURE 3. The two spatial branches after the exchange showing regions of both streamline-curvature and crossflow instability at $\theta = 10^\circ$ and $R = 2500$.

Figure 4 shows the neutral curves for convective instability in the (R, α_r)- and (R, β)-planes at latitudes of $\theta = 10^\circ$–70°. Each curve encloses a region that is convectively unstable. The neutral curves shown were calculated using the full perturbation equations; while neutral curves calculated using the Orr–Somerfeld equation (2.21) are not shown here, they were found to be single-lobed at each latitude, with critical Reynolds numbers lower than the most dangerous modes in figure 4. The neutral

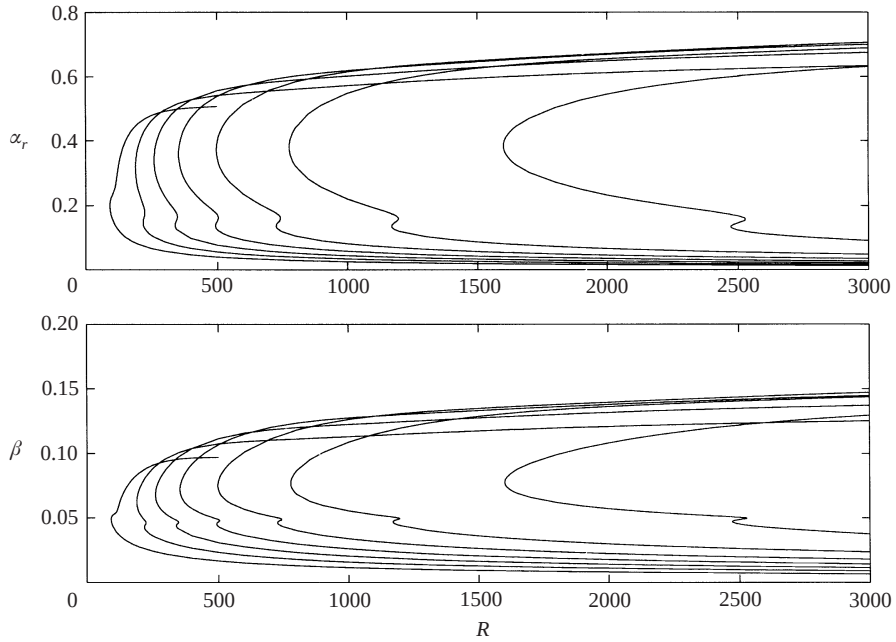

FIGURE 4. The neutral curves of convective instability for stationary vortices at latitudes of $\theta = 10°$–$70°$ (right to left).

curves calculated from the full system and the Orr–Somerfeld equation were found to match for large R, with the discrepancy at low R being reduced with increased latitude.

The neutral curves in figure 4 show that the sphere boundary layer is increasingly stable as we decrease the latitude from the equator towards the pole, consistent with the experimental results of Sawatzki (1970) and Kohama & Kobayashi (1983). At all latitudes in the figure except $\theta = 70°$, a two-lobed structure is seen. The larger lobe, characterized by higher wavenumbers, is due to crossflow instabilities and the smaller lobe, characterized by smaller wavenumbers, is due to streamline-curvature instabilities. The crossflow mode possesses the lowest critical Reynolds number at moderate θ, but the streamline-curvature mode becomes increasingly important as we approach $\theta = 66°$ from below. At $\theta = 66°$ the streamline-curvature mode becomes dominant, and so for $\theta = 70°$ we see a single-lobed neutral curve formed from the streamline-curvature mode. The crossflow mode is seen to distort the shape of the lobe but does not form a lobe itself.

Malik (1986) and Lingwood (1995), in their investigations on the rotating disk, use a Reynolds number based on the local disk velocity at the radius under investigation and the local boundary-layer thickness. The equivalent Reynolds number in our investigation is written as $R_L = R\sin\theta$. Using this Reynolds number a comparison between our results and those of Malik (1986) for the rotating disk are made. Although not shown here, plots of the neutral curves at $\theta = 10°$ in the (R_L, α_r)- and (R_L, β)-planes are very similar to Malik's neutral curves. Figure 5 shows that the convective-instability critical Reynolds numbers of the rotating-sphere boundary layer approach those of the rotating disk as the pole is approached, i.e. as $\theta \to 0$.

For a comparison with the theoretical neutral curves of Taniguchi *et al.* (1998) we consider our results in the (R_S, n)-plane. Here $R_S = \Omega^\star(a^\star)^2/\nu^\star = R^2$ is the spin

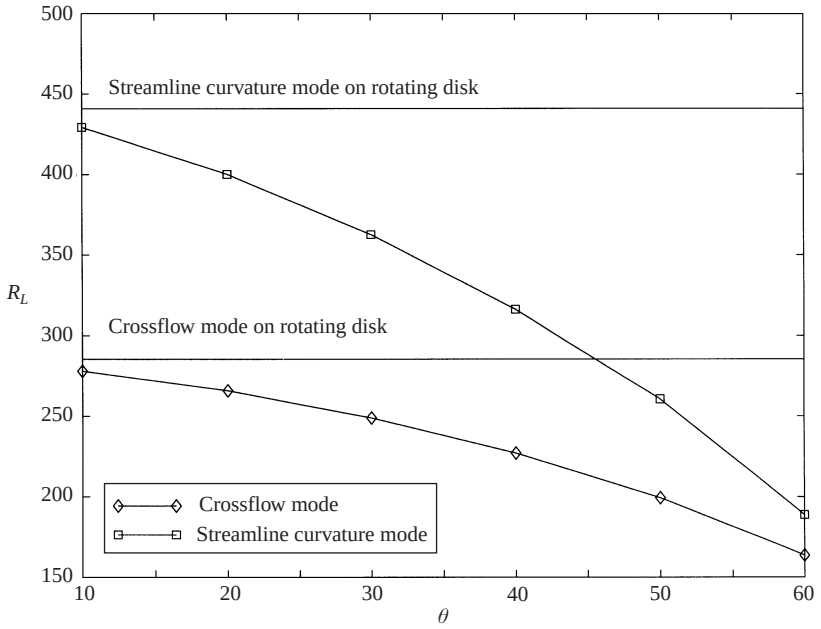

FIGURE 5. A comparison of the critical R_L values for convective instability at each latitude with those of Malik (1986) for the rotating disk (horizontal lines).

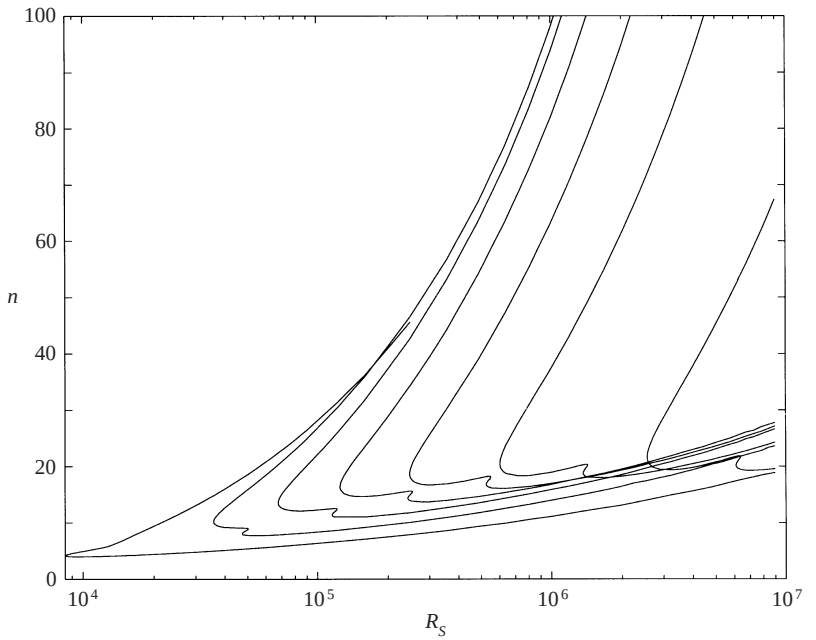

FIGURE 6. The neutral curves of convective instability in the (R_S, n)-plane for stationary vortices at $\theta = 10°$–$70°$ (right to left).

Reynolds number (formed using the sphere radius $a^\star$ as the length scale rather than $\delta^\star$) and n is the number of vortices from (2.20). Figure 6 shows the neutral curves in this plane, where we see that the number of spiral vortices at the onset of instability decreases with increased latitude. This property was also found by Taniguchi *et al.*,

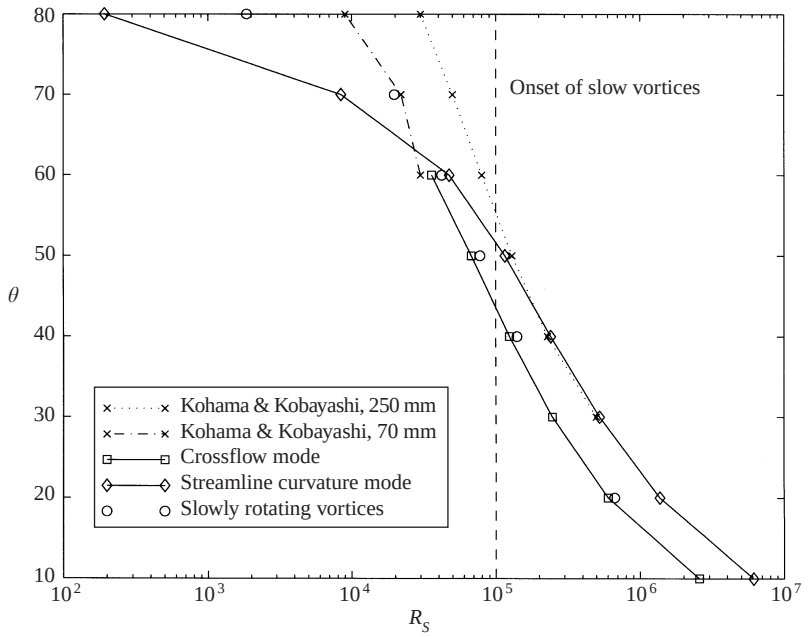

FIGURE 7. The critical Reynolds numbers predicted for stationary vortices, vortices rotating at 0.76 times the sphere surface speed and those experimentally measured by Kohama & Kobayashi (1983). The vertical dashed line indicates the observed onset of vortices rotating at 0.76 times the sphere surface by Kobayashi & Arai (1990).

with the values of n and the critical Reynolds numbers similar to ours. Kohama & Kobayashi (1983) observe the number of spiral vortices at the onset of instability increasing with increased rotation rate, i.e. increased R_S, and tending to the value observed on the rotating disk ($n \approx 32$). Figure 6 is consistent with this behaviour although we find n tending to approximately 22 at the onset of the crossflow mode as we move towards the pole, i.e. the value of n associated with the smallest value of R_S on the upper right-most neutral curve in figure 6. This discrepancy occurs because the spiral vortices are not neutral but growing spatially in the latitudinal direction. The calculated value of n is equal to that calculated by Malik (1986) for the rotating disk. Using (2.19), the vortex angles show a roughly constant value of $\epsilon \approx 11.4^\circ$ and 19.4° at the onset of the crossflow and streamline-curvature instability modes respectively at all latitudes. This is consistent with the results of Malik (1986) on the rotating disk, where the vortex angles are calculated to be $\epsilon = 11.4^\circ$ and 19.5° respectively, and are reasonably close to the experimental observation of $\epsilon \approx 14^\circ$ reported by Kohama & Kobayashi (1983) on the rotating sphere. Taniguchi *et al.* fail to observe the streamline-curvature instability lobe in their neutral curves for latitudes lower than $\theta = 40^\circ$. The explanation for this must arise from the approach taken in their calculations. Recall that they fix the vortex angle at 14° which is in contrast to the approach taken in this paper where the speed of the spiral vortices is fixed with respect to the surface rotation speed of the sphere.

In figure 7, a comparison is made between the predicted critical Reynolds numbers calculated using the stationary-vortex assumption and the experimental results of Kohama & Hobayashi (1983). For latitudes lower than $\theta = 60^\circ$ we see very good agreement between the experimental critical Reynolds numbers of Kohama & Kobayashi's larger sphere and the predicted onset of streamline-curvature instabilities.

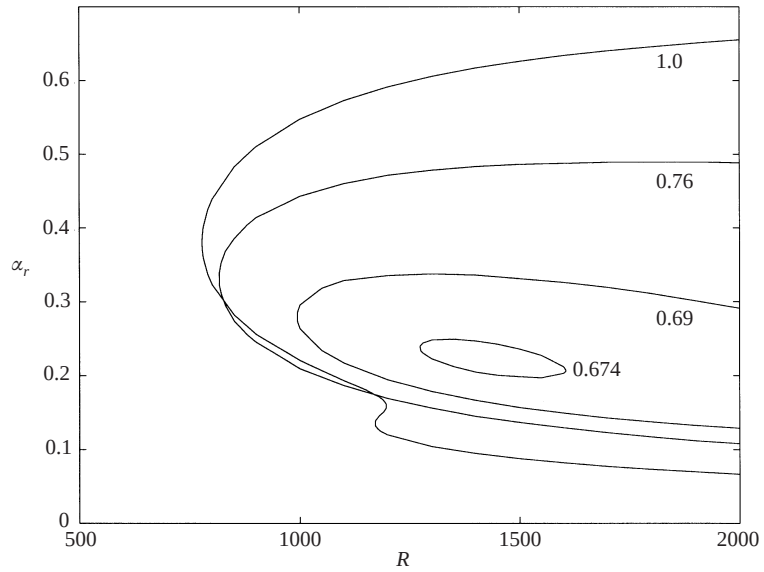

FIGURE 8. Neutral curves for convective instability in the (R, α_r)-plane at $\theta = 20^\circ$ calculated for vortices rotating at speeds of 1.0, 0.76, 0.69 and 0.674 times the surface speed of the sphere.

This is unexpected as the experiments should measure the lowest critical Reynolds numbers and so pick up the onset of crossflow instabilities at latitudes below $\theta = 66^\circ$. However, note that Kohama & Kobayashi's critical Reynolds numbers for their smaller sphere do match onto the predicted onset of crossflow instabilities, although unfortunately the critical Reynolds numbers for $\theta < 60^\circ$ appear not to have been measured on the smaller sphere. These findings may suggest that different instability modes were being measured on the different sized spheres. Further experimental investigations are required to clarify this. At a latitude of $\theta = 60^\circ$ we see a discrepancy between the experimental critical values and those predicted for stationary vortices, and this discrepancy quickly increases beyond this latitude. Note that this behaviour is similar to that found by Taniguchi *et al.*, and starts at the Reynolds number measured by Kobayashi & Arai for the onset of the slow vortices. This strongly suggests that the discrepancy is due to the stationary vortex assumption being invalid at higher latitudes, and this point will be addressed now.

3.2. *Slowly rotating vortices*

The convective instability of the boundary layer has been studied for a variety of vortex speeds at a number of latitudes. The neutral curves at each of these latitudes show a similar behaviour as the vortex speed is reduced, i.e. the streamline-curvature lobe is smoothed out as the speed is decreased, producing a single-lobed neutral curve. The critical Reynolds numbers are found to increase with reductions in the vortex speed, with the neutral curve eventually closing up and disappearing below a critical value. This means that the boundary layer is increasingly stable to slowly rotating vortices and cannot support them below a certain value of vortex speed. The critical vortex speed has been found to decrease with latitude. Figure 8 shows the set of neutral curves at a latitude of $\theta = 20^\circ$, but the behaviour is typical of all latitudes. Figure 7 shows the results of the slow vortex assumption analysis (i.e. speed 0.76 times the sphere surface speed). By considering slowly rotating vortices the

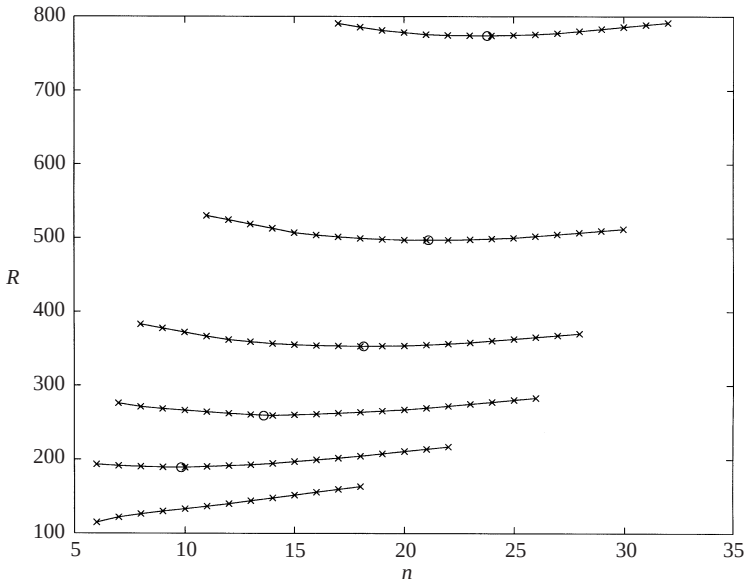

FIGURE 9. Critical Reynolds numbers at latitudes of $\theta = 20°$–$70°$ (top to bottom) for neutral curves defined by fixing n at various integer values. The circles indicate the results of § 3.1.

discrepancy between the experimental and predicted results is removed at $\theta = 70°$, and greatly reduced at $\theta = 80°$.

To further investigate the vortex speed another approach can be taken in which we plot the neutral curves defined by $\gamma_i = \alpha_i = 0$ that correspond to each integer n. The global neutral curve at a particular latitude would then be the envelope of the neutral curves pertaining to each single n. This approach does not require us to fix the longitudinal wave speed c, but allows its prediction from the critical values of γ_r and R using $c = \gamma_r R \sin\theta / n$. This approach has been taken at latitudes in the range $\theta = 20°$–$70°$ in $10°$ increments and the critical values of R for various integer n are shown in figure 9.

At $\theta \leqslant 60°$ we see that the curves have a single minimum. This minimum is the critical Reynolds number of the crossflow lobe of the enveloping neutral curve, and is identical to that calculated in § 3.1 when c was fixed at unity. The points where $c = 1.0$ for each θ are also indicated on figure 9. The critical values of γ_r and R at the minimum in the curve at each latitude lead to the prediction that $c \approx 1.0$. This agreement shows that fixing the longitudinal wave speed to $c = 1.0$ at the low latitudes, as was done in § 3.1, is correct. This is in full agreement with the experimental results of Kohama & Kobayashi (1983).

Figure 9 also shows that as the latitude is increased the curves flatten out until at $\theta = 70°$ an inflection point is seen rather than the minimum. Further investigation of latitudes between $\theta = 60°$ and $70°$ have shown that the inflection point first appears at $\theta = 66°$. This is the latitude at which the streamline-curvature mode becomes dominant. Hence, for $\theta \geqslant 66°$, our approach predicts that stationary vortices no longer occur. However, since for $\theta \geqslant 66°$ figure 9 does not predict a minimum critical R, we are not able to fix the value of the longitudinal wave speed at these high latitudes from our theory. The value $c = 0.76$, which we applied earlier in this section, has to be taken from experiment.

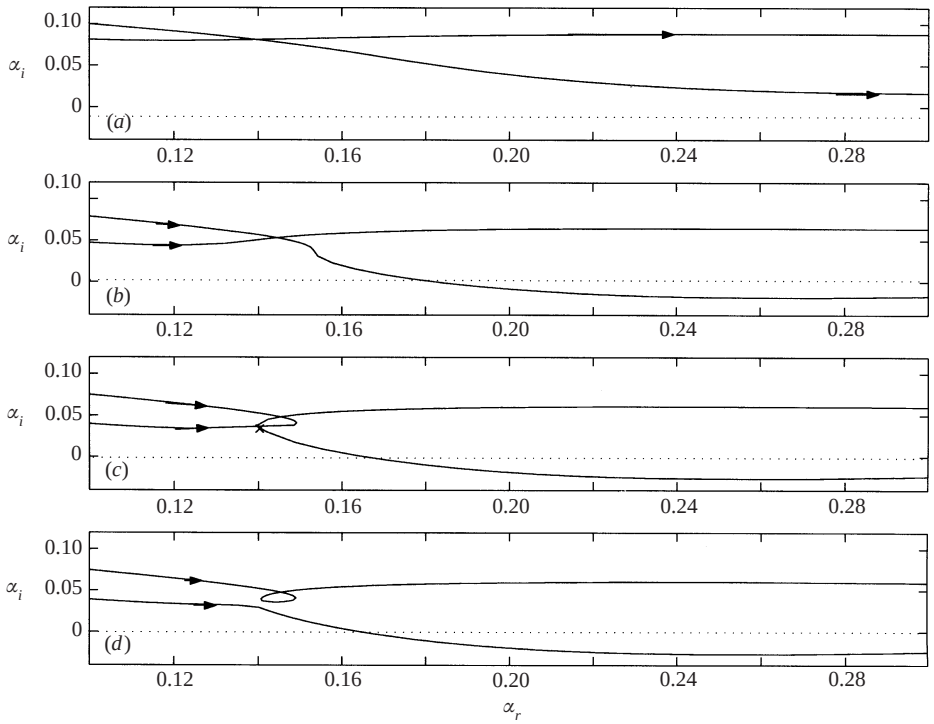

FIGURE 10. Branches of type 1 and 2 at $\theta = 70°$ when $R = 150$, $n = 9$ and (*a*) $\gamma_i = 3 \times 10^{-3}$, (*b*) 1×10^{-4}, (*c*) -4.146×10^{-4} and (*d*) -4.5×10^{-4}. The branch point is indicated by $\times$.

4. The absolute instability analysis

In this section we solve the perturbation equations (2.13)–(2.18) subject to the boundary conditions (3.1) with the aim of studying the occurrence of absolute instabilities. To enable a spatio-temporal analysis to be completed, α and γ are both complex quantities, while β remains real in order to enforce periodicity round the azimuth. The term 'spatial branch' will be used again but this time to refer to solutions of the dispersion relation that lie in the α-plane and have complex γ.

Briggs' criterion, see Briggs (1964), is applied with fixed β to distinguish between convectively and absolutely unstable time-asymptotic responses to an initial boundary-value perturbation. The perturbation is provided by an impulsive longitudinal line forcing, $\delta(\theta - \theta_s)\delta(t)\mathrm{e}^{\mathrm{i}n\phi}$, where $\delta(\theta - \theta_s)$ and $\delta(t)$ are the Dirac delta functions at the latitude θ_s and at time $t = 0$ respectively. The criterion for absolute instability requires branch-point singularities between at least two spatial branches of the dispersion relation. Two of these branches must lie in distinct half-α-planes when γ_i is sufficiently large and positive. Such a singularity is known as a pinch point. If $\gamma_i > 0$ at the pinch point the flow is absolutely unstable, otherwise the flow is only convectively unstable or stable. The latitudinal group velocity $\partial\gamma/\partial\alpha$ is identically zero at a pinch point. A branch-point singularity between two spatial branches that lie in the same half-α-plane for large positive values of γ_i does not cause absolute instability. The value of γ at a pinch point is denoted by γ° and $\alpha(\gamma^\circ) = \alpha^\circ$.

By considering the Rayleigh equation, Lingwood (1995) has shown that the absolute instability of the rotating-disk boundary layer is inviscid in origin. By considering the Orr–Somerfeld equation with very high Reynolds number, we have found that this

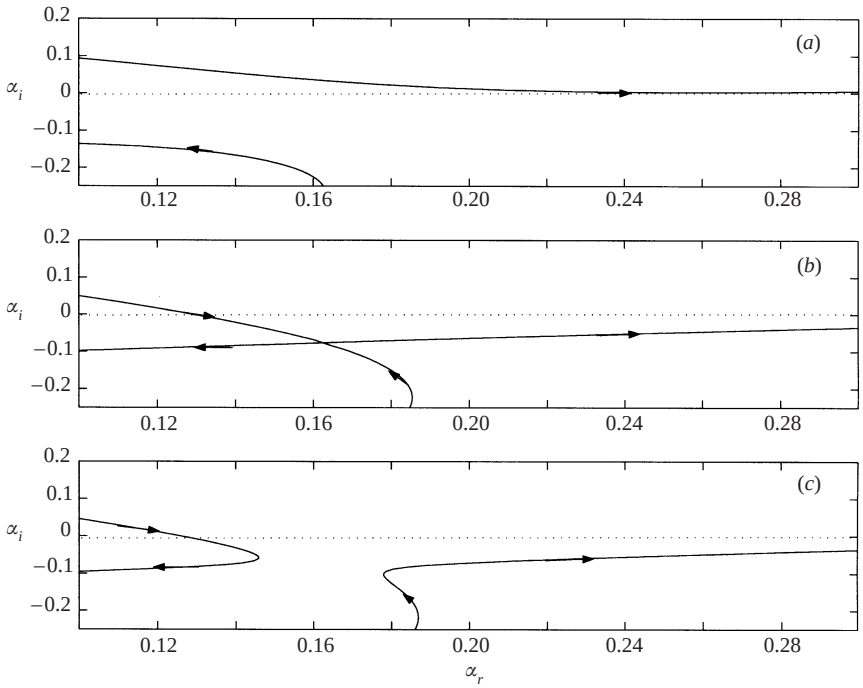

FIGURE 11. Branches of type 1 and 3 at $\theta = 70°$ when $R = 300$, $n = 30$ and (*a*) $\gamma_i = 4 \times 10^{-3}$, (*b*) 1.157×10^{-3} and (*c*) 1×10^{-3}.

is also the case for the rotating sphere at each latitude. For this reason we consider only the full perturbation equations (2.13)–(2.18) in this paper.

Figure 10 shows the progress of branches 1 and 2 with $R = 150$ and $n = 9$ ($\beta = 0.06$) at a latitude of $\theta = 70°$, but is typical of the behaviour for all latitudes. In § 3 it was shown that branches of type 1 and 2 arise from crossflow and streamline-curvature effects respectively. The figure shows the branches when $\gamma_i = 3 \times 10^{-3}$, 1×10^{-4}, -4.146×10^{-4} and -4.5×10^{-4}. A branch point has been found when $\gamma = 4.445 \times 10^{-2} - \mathrm{i}4.146 \times 10^{-4}$ and $\alpha = 0.140 + \mathrm{i}3.377 \times 10^{-2}$ (as indicated in figure 10*c*), but this is not a pinch point as branches 1 and 2 originate in the same half-α-planes for large γ_i, see figure 10(*a*). Branches of type 1 and 2 originate in the upper half-α-plane for all values of the parameters at each latitude and so represent disturbances convecting away from the source towards the equator. To find an absolute instability we therefore need to consider a branch originating in the lower half-α-plane. Such a branch has been found that is equivalent to the branch 3 of Lingwood (1995).

Figure 11 shows the progress of branches 1 and 3 with $R = 300$ and $n = 30$ ($\beta = 0.1$) at $\theta = 70°$. The figure shows the branches when $\gamma_i = 4 \times 10^{-3}, 1.157 \times 10^{-3}$ and 1×10^{-3}. As branches 1 and 3 originate in distinct half-α-planes there is a pinch point at $\gamma^\circ = 6.652 \times 10^{-2} + \mathrm{i}1.157 \times 10^{-3}$ and $\alpha^\circ = 0.163 - \mathrm{i}7.628 \times 10^{-2}$ in figure 11(*b*). Note the branch exchange after the pinch point in figure 11(*c*).

Pinch points with $\gamma_i > 0$ have been found at all latitudes, and so the boundary layer on the rotating sphere is absolutely unstable for certain values of R and β at each latitude. Figure 12 shows the neutral stability curves for absolute instability in the (R, γ_r°)-, (R, α_r°)-, (R, α_i°)- and (R, β)-planes at $\theta = 70°$, the flow being absolutely unstable inside each curve. The shape of these curves is typical for all latitudes and

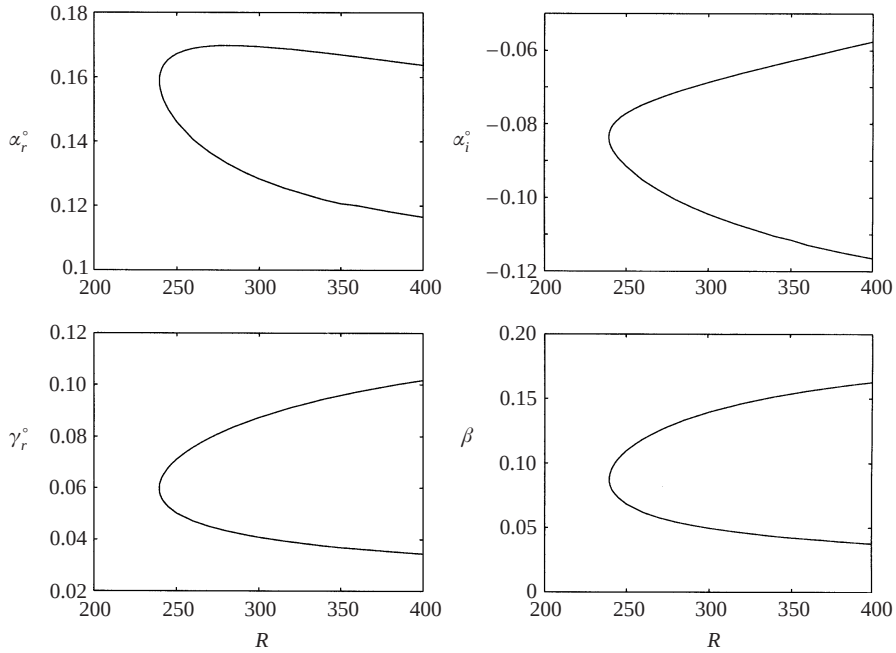

FIGURE 12. Absolute instability neutral curves at $\theta = 70^\circ$ in the (R, α_r°)-, (R, α_i°)-, (R, γ_r°)- and (R, β)-planes.

so we do not show the other neutral curves, but the local critical Reynolds numbers for each latitude are shown in table 1. The local Reynolds number, $R_X = R^2\theta \sin\theta$, is formed using the distance to the latitude in question from the pole over the sphere surface, $a^\star\theta$, as the length scale and the local rotation speed at that point, $a^\star\Omega^\star \sin\theta$, for the velocity scale.

If we convert to the Reynolds number R_L a comparison between our results and those of Lingwood (1995) can then be made. From this we see that the critical values for absolute instability at each latitude approach those of the rotating disk as we move towards the pole. The values of α_r°, α_i° and β in the neutral curve calculated at $\theta = 10^\circ$ show very good agreement with the neutral curves of figure 8 in Lingwood (1995) for the rotating disk, although the values of γ_r° are different due to the differing frames of reference used.

Figure 13 shows a comparison between the predicted onset of absolute instability and the experimentally measured transition points from Kohama & Kobayashi (1983), using the local Reynolds number R_X at each latitude. For latitudes up to and including $\theta = 70^\circ$ the experimental results show that transition occurs at roughly the same local Reynolds number at each latitude, despite the instability waves first appearing across a wide parameter range with varying rotating rate and sphere radius. This observation leads us to expect that the underlying transition mechanism here is an absolute instability. At $\theta = 80^\circ$ we see the transition point at a rather lower local Reynolds number, perhaps indicating that the underlying mechanism is different at high latitudes. The predicted onset of absolute instability is seen to match onto the experimental value well at a latitude of $\theta = 30^\circ$. At this latitude the experimental value is $R_X = 2.2 \times 10^5$ but it should be noted that all experimental data used have simply been read off the graphical results of Kohama & Kobayashi (1983) and so must be considered to be approximate. Beyond this latitude the discrepancy

θ (deg.)	R	R_X
10	2879.81	2.51×10^5
20	1413.10	2.39×10^5
30	912.10	2.18×10^5
40	650.31	1.90×10^5
50	480.63	1.54×10^5
60	352.21	1.13×10^5
70	239.50	6.59×10^4
80	115.39	1.83×10^4

TABLE 1. Values of the Reynolds number R and local Reynolds number R_X at the onset of absolute instability at each latitude θ.

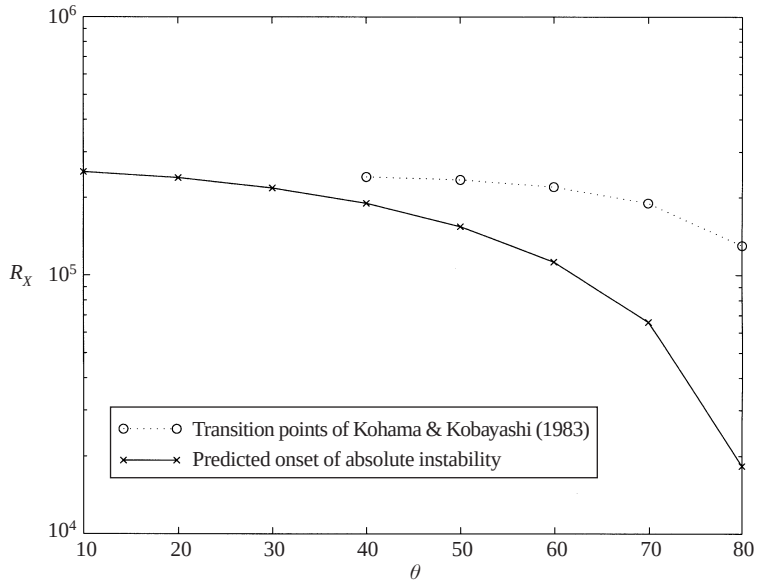

FIGURE 13. A comparison of the predicted critical R_X values for absolute instability with the transitional R_X values measured by Kohama & Kobayashi (1983).

increases, but still remains relatively small below $\theta = 70°$, again perhaps indicating that the transition mechanism may not be an absolute instability at the highest latitudes.

We have now seen that the results of both the convective and absolute instability analyses show a large discrepancy at $\theta = 80°$ when compared to experimental results. Another explanation for the discrepancies is that this latitude may be sufficiently close to the boundary-layer eruption at the equator for the boundary-layer approximations to be invalid.

A consequence of the fact that pinch points occur only between branches that originate in distinct halves of the α-plane is that the total number of crossings of the real axis must be odd (Kupfer, Bers & Ram 1987). It follows that an absolutely unstable region must be surrounded by a region in which one mode is convectively unstable on one side of the source and the other mode stable in the opposite direction.

5. Conclusion

In this paper the rotating sphere was considered in a fixed frame of reference. This formulation has been used in all previous theoretical investigations on the rotating-sphere boundary layer, but is in contrast to the related work of Lingwood (1995) on the rotating disk. In Lingwood's work a frame of reference fixed on the rotating disk is used, resulting in Coriolis terms in the mean-flow and perturbation equations. Apart from the Coriolis terms, the equations governing the rotating sphere are similar to those of the rotating disk. It is known that the mean-flow profiles of the rotating-sphere boundary layer reduce to those of the rotating disk near to the pole, see White (1991). Our investigation shows that the neutral curves for both convective and absolute instability of the boundary layer on the rotating sphere approach those of the rotating disk as we approach the pole. The convective instability neutral curves of Taniguchi *et al.* (1998) do not do this and we expect that this is due to the different approach taken in their calculations.

The convective instability analysis shows that crossflow instabilities dominate below $\theta = 66^\circ$, whilst streamline-curvature instabilities dominate above this latitude due to a region of reverse flow in the radial component of the mean flow. For latitudes lower than $\theta = 60^\circ$ we see very good agreement between the experimental critical Reynolds numbers of Kohama & Kobayashi (1983) and the predicted onset of streamline-curvature instabilities for stationary vortices. However, the critical Reynolds numbers for experiments conducted on a smaller sphere match onto the predicted onset of crossflow instabilities. This suggests that different instability modes were being measured by Kohama & Kobayashi on the different sized spheres. Above a latitude of $\theta = 60^\circ$ we see discrepancies between the experimental critical values and those predicted by assuming stationary vortices. These discrepancies start at the Reynolds number measured by Kobayashi & Arai (1990) for the onset of vortices rotating at 0.76 times the sphere surface speed, and are greatly reduced when we consider vortices rotating at this slower speed. However, a discrepancy still remains at $\theta = 80^\circ$. Using a different approach in the analysis we have shown that the occurrence of the slowly rotating vortices may be associated with the first point at which the streamline-curvature mode becomes dominant, i.e. $\theta = 66^\circ$. However, we are not able to fix the slower longitudinal wave speed at the high latitudes from this theory.

The number of spiral vortices at the onset of instability is predicted to decrease with increased latitude, which is consistent with the observations of Kohama & Kobayashi. As the analysis moves towards the pole we predict that the number of spiral vortices approaches $n \approx 22$, the theoretical prediction for the rotating disk (Malik 1986). This value differs from the experimental observations for both the sphere and the disk of $n \approx 31$ because the spiral vortices are not neutral but growing spatially in the latitudinal direction. At the onset of instability the stationary vortices at each latitude were predicted to have roughly the same vortex angles for each mode, the values found being $\epsilon \approx 11.4^\circ$ and 19.4° at the onset of crossflow instabilities and streamline-curvature instabilities respectively. These values agree well with those of the rotating disk, and are reasonably close to the experimentally observed value of $\epsilon \approx 14^\circ$ on the rotating sphere.

Expressing the observed transition points of Kohama & Kobayashi (1983) in terms of a local Reynolds number, we find that transition occurs at roughly the same value at all latitudes up to and including $\theta = 70^\circ$. At $\theta = 80^\circ$ the transition point is slightly lower. Throughout the paper we have tried to associate transition with the onset of absolute instability, and the predicted onset of the latitudinal absolute instability is seen to match onto the experimental value well at a latitude of $\theta = 30^\circ$. Beyond this

the discrepancy increases but still remains small when below $\theta = 70°$. The theoretical results show that the transition mechanism for the boundary layer on a rotating sphere may be an absolute instability in the latitudinal direction for latitudes up to $\theta = 70°$. Beyond this latitude the absolute instability may be suppressed and other transition mechanisms apply.

Both the convective and absolute instability results show a large discrepancy at $\theta = 80°$. The boundary layer is known to erupt at the equator causing the boundary-layer assumptions to be invalid there; $\theta = 80°$ may be close enough to be affected by this, giving an explanation for these discrepancies.

In the derivation of the governing equations, factors

$$1/(1 + \eta/R), \tag{5.1}$$

that multiplied terms in the perturbation equations have been replaced by unity. This approximation is similar to the parallel flow approximation found in many other boundary-layer investigations and, after conducting the stability analyses, we are now in a position to comment on the validity of the approximation at low and high latitudes. As shown in figure 1, at low latitudes the boundary layer is seen to be fully developed at around $\eta = 5$ but at higher latitudes it is seen to be fully developed only above $\eta = 10$. This thickening of the boundary layer, together with the fact that the critical Reynolds numbers for each type of instability decrease with increased latitude, means that our approximation is less valid near to the equator. The inaccuracy is smallest near to the pole where, at $\theta = 10°$, the onset of convective instability occurs above $R = 1500$. This means that close to the pole the factor (5.1) is approximated by unity with an inaccuracy of about 0.3%. At $\theta = 70°$ the convective instability in the analysis of slow vortices has a critical Reynolds number of around $R = 150$. Here we see that the factor (5.1) is approximated by unity with an error of around 6.7%. For the absolute instability calculations at this latitude the inaccuracy is around 4%. Although the inaccuracy caused by this approximation grows substantially as the analysis moves towards the equator, it is the authors' opinion that it is still not sufficiently large to affect the conclusions of this work.

A number of open issues remain. For instance, more experiments will be required in order to investigate the validity of some of the predictions made here, not least the possible role of absolute instability in the transition (in much the same way as was carried out by Lingwood 1997), but also measurement of the critical Reynolds number for 'slow' vortices at lower latitudes. Additional effects also need to be included in our analysis, such as the presence of axial flow and the behaviour of more general bodies of revolution, and work is well under way in this direction. Further, the relationship between our linear results and the occurrence of nonlinear global modes, as recently found by Pier & Huerre (2001), needs to be explored. Pier & Huerre describe the appearance of nonlinear fronts at the boundary between convective instability upstream and absolute instability downstream, which of course matches the structure of the linear stability found here on the rotating sphere, and indeed by Lingwood on the rotating disk. The possibility of such a nonlinear wave undergoing some secondary instability, to lead to transition, requires careful study.

S. J. G is grateful for the help and guidance given by Dr R. J. Lingwood in the completion of this work, which was supported by the Engineering and Physical Sciences Research Council and the Newton Trust of Cambridge University. Both authors wish to acknowledge the advice given by an anonymous referee in relation to figure 9.

REFERENCES

Banks, W. H. H. 1965 The boundary layer on a rotating sphere. *Q. J. Mech. Appl. Maths* **18**, 443–454

Banks, W. H. H. 1976 The laminar boundary layer on a rotating sphere. *Acta Mech.* **24**, 273–287

Bers, A. 1975 Linear waves and instabilities. In *Physique des Plasmas* (ed. C. DeWitt, J. Peyraud), pp. 117–215. Gordon & Breach.

Briggs, R. J. 1964 *Electron-Stream Interaction with Plasmas*. MIT Press.

Howarth, L. 1951 Note on the boundary layer on a rotating sphere. *Phil. Mag.* **42**, 1308–1315.

Huerre, P. & Monkewitz, P. A. 1985 Absolute and convective instabilities in free shear layers. *J. Fluid Mech.* **159**, 151–168.

Ito, N. 1996 Simple cases of streamline-curvature instability in three-dimensional boundary layers. *J. Fluid Mech.* **317**, 129–154.

Kobayashi, R. & Arai, T. 1990 Spiral vortex behaviour in transition region and separation of three-dimensional boundary layers on spheres rotating in axial flow. In *Laminar Turbulent Transition, IUTAM Symposium Toulouse, France* (ed. D. Arnal & R. Michel), pp. 551–557. Springer.

Kobayashi, R., Kohama, Y., Arai, T. & Ukaku, M. 1987 The boundary-layer transition on a rotating cone in axial flow with free-stream turbulence. *JSME Intl J.* **30**, 423–429.

Kohama, Y. 1984 Behaviour of spiral vortices on a rotating cone in axial flow. *Acta Mech.* **50**, 193–199.

Kohama, Y. & Kobayashi, R. 1983 Boundary-layer transition and the behaviour of spiral vortices on rotating spheres. *J. Fluid Mech.* **137**, 153–164.

Kupfer, K., Bers, A. & Ram, A. K. 1987 The cusp map in the complex-frequency plane for absolute instabilities. *Phys. Fluids* **30**, 3075–3082.

Lingwood, R. J. 1995 Absolute instability of the boundary layer on a rotating disk. *J. Fluid Mech.* **299**, 17–33.

Lingwood, R. J. 1996 An experimental study of absolute instability of the rotating-disk boundary-layer flow. *J. Fluid Mech.* **314**, 373–405.

Lingwood, R. J. 1997 Absolute instability of the Ekman layer and related flows. *J. Fluid Mech.* **331**, 405–428.

Malik, M. R. 1986 The neutral curve for stationary disturbances in rotating-disk flow. *J. Fluid Mech.* **164**, 275–287.

Manohar, R. 1967 The boundary layer on a rotating sphere. *Z. Angew. Math. Phys.* **18**, 320–330.

Niew, T. R. 1993 The stability of the flow in a laminar separation bubble. PhD thesis, Cambridge University.

Peir, B. & Huerre, P. 2001 Nonlinear self-sustained structures and fronts in spatially developing wake flows. *J. Fluid Mech.* **435**, 145–174.

Sawatzki, O. 1970 Das stromungsfeld um eine rotierende Kugel. *Acta Mech.* **9**, 159–214.

Taylor, M. J. & Peake, N. 1998 The long-time behaviour of incompressible swept wing boundary layers subject to impulsive forcing. *J. Fluid Mech.* **355**, 359–381.

Taniguchi, H., Kobayashi, T. & Fukunishi, Y. 1998 Stability of the boundary layer on a sphere rotating in still fluid. *Acta Mech.* **129**, 243–253.

White, F. M. 1991 *Viscous Fluid Flow*. McGraw-Hill.